Fusion studies in $^{16}O + ^{142,150}Nd$ reactions at energies near the Coulomb barrier

A. C. Visakh,[*] E. Prasad,[†] P. V. Laveen, M. Shareef,[‡] and A. Shamlath[§]
Department of Physics, Central University of Kerala, Kasaragod, 671316, India

S. Nath, N. Madhavan, J. Gehlot, Gonika, Rohan Biswas, and A. Parihari
Inter University Accelerator Centre, Aruna Asaf Ali Marg, New Delhi - 110067, India

J. Khuyagbaatar
Helmholtz Institute Mainz, 55099 Mainz, Germany
and GSI Helmholtzzentrum für Schwerionenforschung GmbH, D-64291 Darmstadt, Germany

B. Lommel and B. Kindler
GSI Helmholtzzentrum für Schwerionenforschung GmbH, D-64291 Darmstadt, Germany

A. M. Vinodkumar, B. R. S. Babu, and S. Sanila
Department of Physics, University of Calicut, Calicut, 673635, India

K. M. Varier
Department of Physics, University of Kerala, Thiruvananthapuram, 695034, India

S. Appannababu
Department of Nuclear Physics, Andhra University, 530003, India

(Received 3 June 2021; accepted 30 September 2021; published 3 November 2021)

Background: Enhancement in fusion cross sections over one-dimensional barrier penetration model (1D-BPM) predictions has been observed at sub-barrier energies owing to the coupling of various internal degrees of freedom to the relative motion. On the other hand, hindrance in fusion is noticed at energies well above the barrier in a few cases.
Purpose: The purpose is to probe the dynamics of heavy ion fusion at energies below and well above the Coulomb barrier.
Methods: Fusion excitation functions for the $^{16}O + ^{142,150}Nd$ reactions are measured using the Heavy Ion Reaction Analyzer (HIRA) at IUAC, New Delhi. Measurements have been performed in the range 12% below to 50% above the Coulomb barrier for both systems. The measured fusion cross sections are compared with coupled channels calculations using CCFULL code. The cross sections are also compared with reactions using ^{16}O beams with other isotopes of Nd to explore the systematic behavior of fusion.
Results: Compared with 1D-BPM predictions, fusion enhancement is observed in both $^{16}O + ^{142}Nd$ and $^{16}O + ^{150}Nd$ reactions at below-barrier energies, with the latter reaction showing a higher enhancement. Coupled channels calculations incorporating the collective excitations of the target nuclei reproduce the fusion cross sections in both reactions. The collective excitations of the projectile nucleus do not seem to contribute to the observed fusion enhancement. Calculations using Akyüz-Winther potential parameters fail to reproduce the fusion cross sections at energies well above the barrier.
Conclusions: Fusion enhancement is observed in both reactions studied. Degree of enhancement of sub-barrier fusion cross section is larger for the reaction using ^{150}Nd target. Fusion hindrance is observed in both reactions at very high energies. The hindrance seems to increase with increasing beam energy. Larger value of diffuseness parameter compared with the value consistent with elastic-scattering measurements is required to reproduce the

[*]acvisakh@gmail.com
[†]Corresponding author: prasadenair@cukerala.ac.in
[‡]Present address: Nuclear Physics Division, DAE-Saha Institute of Nuclear Physics (SINP), 1/AF, Saltlake, Kolkata, West Bengal-700064, India.
[§]Present address: Institute for Integrated Programmes and Research in Basic Sciences (IIRBS), Mahatma Gandhi University, Kottayam, 686560, India.

fusion excitation function at energies well above the barrier. This could be a strong indication of dynamical effects in fusion at very high energies.

DOI: 10.1103/PhysRevC.104.054602

I. INTRODUCTION

Being the only established pathway towards the *island of stability* [1–4], heavy ion fusion is a topic of significant interest in modern physics research. Fusion is characterized by the formation of the equilibrated compound nucleus (CN) [5] which may be formed by overcoming the Coulomb barrier or tunneling through the barrier. Although fusion at energies above the Coulomb barrier can be explained using classical treatments, the dynamics become increasingly complicated at sub-barrier energies where quantum effects are significant. It is known that fusion cross sections are significantly enhanced at sub-barrier energies compared with the 1D-BPM calculations [6–11]. 1D-BPM calculations only account for the relative motion degree of freedom of the reacting nuclei during the tunneling. It is now well known that the coupling of various internal degrees of freedom of the colliding nuclei such as static deformation [11–13], collective vibration [14–16], nucleon transfer channels [17–19], etc. contribute to the observed enhancement in fusion cross sections [8,13] at sub-barrier energies. These couplings lead to a distribution of barriers [20–22] and favor fusion at sub-barrier energies.

Sub-barrier fusion studies provide ideal platform for exploring the dynamics of many-body quantum systems. Although coupled channels (CC) formalism is quite successful in establishing the role of static deformation and vibrational degrees of freedom in sub-barrier fusion cross section enhancement, the exact nature of transfer channels is not known to complete satisfaction until date. It was shown that neutron transfer channels with positive Q-value enhance sub-barrier fusion cross sections [23–28], particularly for the one neutron and two neutron transfer channels [29]. Such enhancement has relevance in superheavy element synthesis as well, where neutron-rich radio active beams could be used as projectiles at near-barrier energies.

However, no noticeable enhancement is observed in projectile-target combinations like ^{58,64}Ni + ^{130}Te [28], ^{16,18}O + ^{76,74}Ge [30], etc. where neutron transfer channels have positive Q values. It is proposed that the change of deformations of the collision partners with neutron transfer can significantly influence sub-barrier fusion [31–33]. If the deformation of the interacting nuclei are less after the neutron transfer, the enhancement is insignificant even for systems with positive Q value transfer channels.

Despite its success in explaining the cross-section enhancements at near and sub-barrier energies, deviations from CC calculations have been noticed at deep sub-barrier energies as well as at energies much above the Coulomb barrier. Substantial reduction in fusion cross section is observed at deep sub-barrier energies over the predictions of CC theory [34–37]. This hindrance was attributed to a shallower potential due to Pauli's exclusion principle [38–40], tunneling through a thicker barrier characterized by adiabatic one-body potential [41], or to quantum decoherence of the channel wave functions [37,42] in different proposals.

Another problem is encountered at very high energies—much above the Coulomb barrier—where quantum tunneling does not play any significant role. It has already been noticed that the barrier distribution and fusion cross sections well above and below the average barrier cannot be reproduced simultaneously [43] using the same set of potential parameters V_0, r_0, and a in CC calculations, where V_0 is the depth of the potential well, r_0 is the radius parameter, and a is the surface diffuseness parameter, respectively. A larger value of a (between 0.75 and 1.5) is needed to fit the cross section well above the barrier [44–47] compared with the value ($\approx$0.65) obtained from elastic-scattering experiments [48,49]. A systematic study of a number of reactions [44] reported that the values of a increase with increase in $Z_P Z_T$, where Z_P and Z_T are the atomic numbers of the projectile and target nuclei, respectively. The observed *fusion hindrance* at higher energies is attributed to the dynamical effects in some works. Dynamical effects are not included in CC calculations. Questions are also raised on the appropriateness of Woods-Saxon form of the potential used in the CC calculations. The exact reason for this observation is not yet known and warrants more cross section measurements at energies well above the barrier.

We report fusion excitation function measurements for the ^{16}O + ^{142,150}Nd systems forming compound nucleus ^{158,166}Er in this work. The reactions studied have significant similarities with the well-explored ^{16}O + ^{A}Sm systems. ^{142}Nd is similar to ^{144}Sm—less deformed ($\beta_2 = 0.088$ for ^{144}Sm and 0.091 for ^{142}Nd), and singly magic ($N = 82$). ^{150}Nd is a deformed nucleus ($\beta_2 = 0.285$) with well-defined rotational bands like ^{154}Sm ($\beta_2 = 0.339$). Both ^{16}O + ^{A}Nd and ^{16}O + ^{A}Sm reactions have no neutron transfer channels with positive Q value.

The measurements span the energy range of $\approx$12% below to $\approx$50% above the Coulomb barrier for both the reactions. Surprisingly, a larger value of diffuseness parameter was required to reproduce the fusion excitation function in ^{16}O + ^{A}Sm systems [44] at well above the barrier energies. Values of a also showed a correlation with increasing neutron number of the target nucleus in the oxygen-induced reaction with different isotopes of samarium targets. Hence, it is interesting to explore the dynamics of fusion in ^{16}O + ^{142,150}Nd systems at near and above-barrier energies.

The paper is organized as follows. The experimental details are presented in Sec. II, followed by the data analysis procedure in Sec. III. The results of present investigations and a discussion on our findings are presented in Sec. IV. The paper is summarized and concluded in Sec. V.

II. EXPERIMENTAL DETAILS

The experiment was carried out at Inter University Accelerator Center (IUAC), New Delhi, using the 15 UD Pelletron [50] accelerator. Pulsed beams of ^{16}O, with a pulse

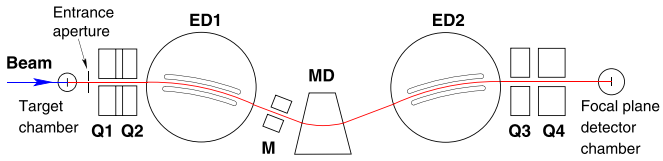

FIG. 1. Schematic representation of HIRA.

separation of 4 μs, was used to bombard the isotopically enriched ^{142}Nd and ^{150}Nd targets of thicknesses ≈140 and ≈162 $\mu g/cm^2$, respectively, evaporated on ≈38 $\mu g/cm^2$ carbon backing. Typical beam current of three particle nanoampere (pnA) was used throughout the experiment for the irradiation of the target, and the irradiation time was decided by the statistics of the ERs detected in the focal plane detectors. The targets were mounted such that the carbon backing faces the beam first. The measurements were performed in the beam energy range of 60 to 104 MeV and 56 to 104 MeV, for the $^{16}O + ^{142}Nd$ and $^{16}O + ^{150}Nd$ reactions, respectively. Energy-loss corrections were applied for the carbon backing as well as for the half-thickness of the target, assuming that the projectile-target interaction happens at the middle of the target. The low-energy ERs produced in the fusion reactions were separated from other possible scattered particles using the Heavy Ion Reaction Analyser (HIRA) [51].

The electromagnetic configuration of HIRA is Q1Q2-ED1-M-MD-ED2-Q3Q4, where Q, MD, M, and ED stand for the magnetic quadrupole, magnetic dipole, magnetic multipole, and electrostatic dipole, respectively [51]. HIRA was set at zero degrees with respect to the beam direction with a solid angle of acceptance of 5 msr (polar angle ≈2.2°) in this study. This arrangement efficiently transports the ERs to the focal plane chamber by dispersing them according to their mass to charge (m/q) value and rejects the intense beam background.

A schematic representation of HIRA is shown in Fig. 1. Two silicon surface barrier detectors (SSBDs) were mounted inside the sliding-seal scattering chamber at $\theta_{lab} = 15.5°$ with respect to the incident-beam direction and used for absolute normalization of the ER cross sections. The elastic yields registered by these detectors were also used to monitor the beam. A 30 $\mu g/cm^2$ thick carbon foil was placed 10 cm downstream from the target to reset the charge state of the ERs after possible internal-conversion processes.

ERs reaching the focal plane were detected by using a position sensitive multiwire proportional counter (MWPC) [52] with active area of 150 mm × 50 mm operated at a pressure of 3.0 mbar of isobutane gas. This MWPC is 8.6 m away from the target mounted in the target chamber. For the unambiguous detection of the ERs, a time-of-flight (ToF) was set up using the radio frequency (rf) signal as the start and MWPC timing signal as the stop. A two-dimensional spectrum of energy loss of the ERs (ΔE) versus ToF for the $^{16}O + ^{142}Nd$ reaction, at 88 MeV beam energy, is shown in Fig. 2. The ERs are shown inside the rectangular gate and are clearly separated from other scattered particles reaching the focal plane detector. This excellent beam rejection capability of HIRA enabled us to measure cross sections down to a few microbarns in this work.

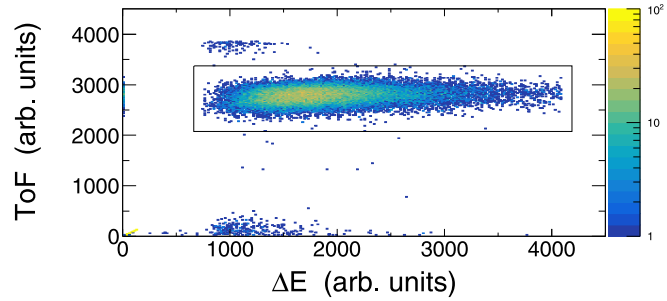

FIG. 2. Two-dimensional ΔE versus ToF spectra for the $^{16}O + ^{142}Nd$ at 88 MeV beam energy. ERs are shown inside the rectangular gate and are clearly separated from other scattered particles reaching the focal plane through multiple scattering.

To maximize the transmission of the ERs reaching the focal plane, HIRA fields were optimized by scanning the mass, charge state, and energy of the most probable ERs, for both reactions, at 88 MeV beam energy. The field values for other energies were scaled from the optimized values obtained at 88 MeV.

III. DATA ANALYSIS

Using the yields of ERs (Y_{ER}) registered at the focal plane detector, ER cross section is calculated using the equation

$$\sigma_{ER} = \frac{Y_{ER}}{Y_{mon}} \left(\frac{d\sigma}{d\Omega}\right)_R \Omega_M \frac{1}{\epsilon_{HIRA}}, \quad (1)$$

where $Y_{mon} = \sqrt{Y_{monL} Y_{monR}}$, with Y_{monL} and Y_{monR} being the yields of the Rutherford scattering events recorded by the left and right monitor detectors, $(\frac{d\sigma}{d\Omega})_R$ is the differential Rutherford scattering cross section at the monitor angle in laboratory frame, Ω_M is the solid angle subtended by each monitor detector and ϵ_{HIRA} is the average ER transmission efficiency of HIRA at the particular energy. The beam is tuned well to ensure that the two monitor detectors count more or less same events throughout the experiment. The geometrical mean $\sqrt{Y_{monL} Y_{monR}}$ ensures the minimum effect of beam fluctuations from zero degree during the run.

The Rutherford scattering cross section in the laboratory frame is calculated using the relation

$$\left(\frac{d\sigma}{d\Omega}\right)_R \simeq 1.296 \left(\frac{Z_P Z_T}{E_{lab}}\right)^2 \left[\frac{1}{\sin^4\left(\frac{\theta_{Lab}}{2}\right)} - 2\left(\frac{M_P}{M_T}\right)^2\right]. \quad (2)$$

The transmission efficiency (ϵ_{HIRA}) is the ratio of the number of ERs reaching the focal plane to the total number of ERs produced at the target center during the reaction. It depends on several reaction-specific and instrument-specific parameters [53], such as entrance channel mass asymmetry, beam energy, target thickness, exit channels of interest, angular acceptance of HIRA, reference particle settings, and size of the focal plane detector. ϵ_{HIRA} is expected to be different at different beam energies.

We calculated the ϵ_{HIRA} using the semimicroscopic Monte Carlo code TERS [54] in this work. TERS generates realistic values of displacement (position), divergence (angle), energy and charge state distribution of the ERs, event by event, and calculates the ER trajectories using first-order ion optical transfer

TABLE I. Experimental ER excitation function (σ_{ER}) for the $^{16}O + ^{142}Nd$ and $^{16}O + ^{150}Nd$ reactions. E is the center-of-mass energy (in MeV) and σ is the cross section (in millibarns).

$^{16}O + ^{142}Nd$			$^{16}O + ^{150}Nd$		
E (MeV)	σ_{ER} (mb)	$\Delta\sigma_{ER}$ (mb)	E (MeV)	σ_{ER} (mb)	$\Delta\sigma_{ER}$ (mb)
93.2	766	116	93.7	1101	166
89.6	767	116	90.1	1103	166
86.0	756	114	86.5	1051	159
82.4	746	112	82.9	1003	152
78.8	767	115	79.3	848	127
76.1	711	107	76.5	740	111
73.4	675	102	73.8	785	119
70.7	574	87	71.1	672	102
68.0	476	71	68.4	538	81
66.2	365	55	66.6	499	75
64.4	282	42	64.8	461	69
62.6	207	31	63.0	391	59
60.8	143	22	61.1	311	47
59.0	55.	8	59.3	177	27
57.2	9	1.4	57.5	71	11
55.4	0.8	0.1	55.7	24	4
53.6	0.03	0.005	53.9	6.4	1.0
			52.1	0.9	0.15
			50.3	0.06	0.001

matrices. The dominant ER channels were simulated using the statistical code PACE3 [55] for both reactions, at all measured energies. ϵ_{HIRA} is calculated for all evaporation channels with relative population more than 1%. The transmission efficiency at a given energy is then obtained from the weighted average of ϵ_{HIRA} values for these channels.

Unambiguous identification of the low-intensity ERs from other possible contaminants reaching the focal plane is a tricky job in all recoil mass spectrometers and separators. Simultaneous measurement of ΔE and the ToF of the particles reaching the focal plane detector helps in the separation of ERs from other scattered events, as shown in Fig. 2. This procedure, however, becomes more challenging with decreasing beam energy, particularly at sub-barrier energies, due to the exponentially falling ER cross sections. On the other hand, Rutherford events increase considerably with decreasing beam energy and the increased beam background overlap significantly with the ER events in the detector at low energies. We followed a similar method discussed by Rajbonshi *et al.* [56]. The two-dimensional scatter plot of ΔE vs ToF is carefully examined to understand the correlation between the ER and Rutherford events as a function of energy. The centroid and full width at half maximum (FWHM) of the ToF projections of both ERs and Rutherford events are analyzed. For this we projected the blob of events to the ToF axis and noted down the centroid and FWHM by fitting Gaussian for both groups of events. It is observed that the difference between the centroids of ER and scattered particle groups increases linearly with decreasing energy. The FWHM of the ER groups is found to increase with decreasing beam energy. At below-barrier energies, where the two groups start to overlap, least-square fit and extrapolation from above-barrier data have been employed as discussed in Ref. [56].

Measured ER cross sections for the two reactions are presented in Table I as a function of center-of-mass (c.m.) energy E. The overall uncertainty includes the statistical uncertainty and the uncertainty in transmission efficiency calculations. Among these, the transmission efficiency contributes the maximum to the total uncertainty.

IV. RESULTS AND DISCUSSION

Measured ER cross sections for the two reactions are shown in Figs. 3(a) and 3(b). As the fission cross sections are negligibly small in the energy range of the present study [57],

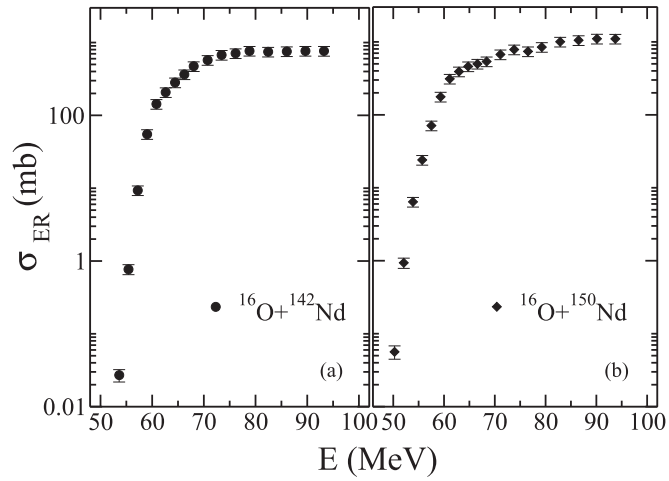

FIG. 3. The experimental ER cross sections of the reactions $^{16}O + ^{142}Nd$ and $^{16}O + ^{150}Nd$ as a function of energy in c.m. frame.

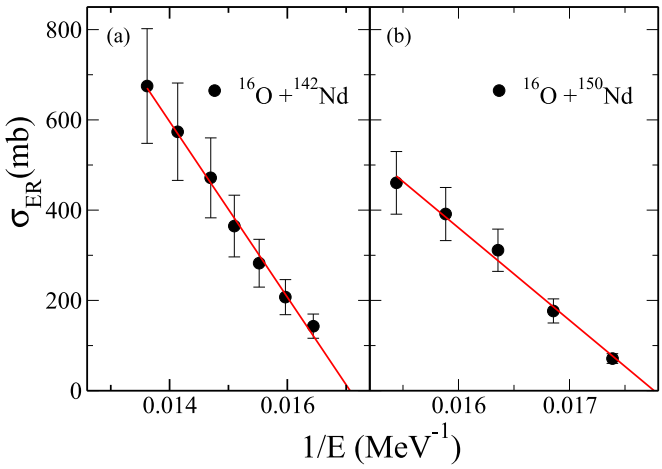

FIG. 4. The experimental fusion cross sections in the energy range $V_b < E < 1.2V_b$ is plotted against the inverse of center-of-mass energy (E). The x intercept of the linear fit gives the inverse of experimental barrier.

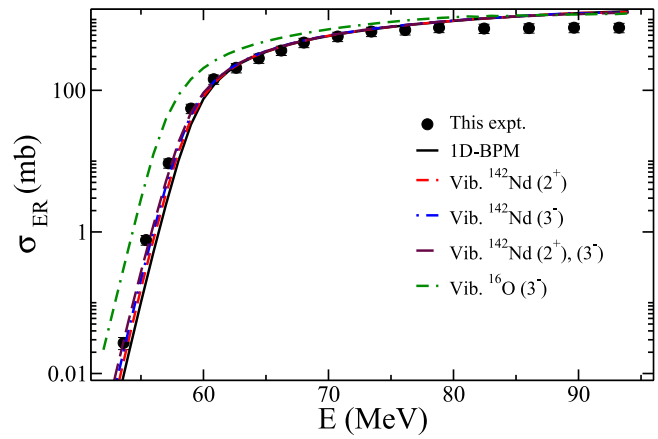

FIG. 5. The experimental fusion excitation function for the $^{16}O + ^{142}Nd$ reaction along with CC calculations.

the total ER cross sections may be treated as the fusion cross sections in these reactions.

A. Coupled channels calculations

Coupled channels code CCFULL [58] has been used to analyze the measured fusion cross sections for the two reactions. The Akyüz-Winther (AW) [59] parametrization of the nuclear potential was used to obtain the potential parameters V_0, r_0, and a in CCFULL calculations. The potential parameters were fixed by reproducing the experimental Coulomb barrier.

Classically, the fusion cross section is given by $\sigma_{\rm fus}(E) = \pi R_b^2(1 - \frac{V_b}{E})$, where R_b is the barrier radius. For obtaining the experimental barrier height (V_b), fusion cross sections (on a linear scale) are plotted against the inverse of center-of-mass energy E, as shown in Fig. 4. The x intercept of the linear fit of the cross section is used to get the experimental barrier. Although the measured fusion cross sections span $0.88V_b < E < 1.5V_b$, cross sections in the energy range $V_b < E < 1.2V_b$ were used for calculating the experimental fusion barrier, for the following reasons: First of all, at $E > V_b$, channel coupling effects are negligible and the classical expression for fusion cross section holds good. This is not true for sub-barrier energies, where coupling effects are important. However, at energies well above the Coulomb barrier, the suppression of fusion cross sections is observed compared with the classical estimates in a few cases [37,44]. Hence, a safer energy range, free from channel coupling effects and dynamical effects [44], is chosen for obtaining the experimental barrier for the systems under study. Experimental barrier V_b and the potential parameters used in CCFULL for the two reactions are presented in Table II.

The effects of various intrinsic degrees of freedom on fusion cross sections have been incorporated in the coupled channels calculations, as discussed below.

1. $^{16}O + ^{142}Nd$ *reaction*

Calculations have been carried out with and without incorporating the couplings, using the AW potential parameters $V_0 = 65$ MeV, $r_0 = 1.19$ fm, and $a_0 = 0.65$ fm. It may be noticed that 1D-BPM calculations considering the reacting nuclei as inert underestimate the sub-barrier fusion cross sections, as shown by the black solid line in Fig. 5.

Coupled channels calculations with different inelastic excitations of the projectile and target nuclei are shown in Fig. 5. Being a semimagic nucleus, the degree of collectivity expected for the ^{142}Nd is small. Calculations considering the projectile as inert and the vibrational coupling of 2^+ state of ^{142}Nd underestimate the cross sections at sub-barrier energies. A similar calculation considering the 3^- state of ^{142}Nd also fails to reproduce the sub-barrier cross sections in this case. Significant enhancement in the cross sections and a reasonable agreement with the experimental values have been noticed when both 2^+ and 3^- states (one-phonon coupling) of ^{142}Nd were coupled with the relative motion degrees of freedom. The details of the coupling parameters used are given in Table III.

TABLE II. The AW potential parameters (V_0, r_0, a) and the resulting barrier parameters (V_b, R_b, $\hbar\omega$) used in the CC calculations for the $^{16}O + ^{142,150}Nd$ reactions. The experimental barrier and Swiatecki barrier [60] are also shown.

Reaction	V_0 (MeV)	r_0 (fm)	a (fm)	V_b (MeV)	R_b (fm)	$\hbar\omega$ (MeV)	V_b (Expt) (MeV)	R_b (Expt) (fm)	V_b (Swiatecki) (MeV)
$^{16}O + ^{142}Nd$	65	1.19	0.65	59.0	10.98	4.40	58.59	10.27	58.83
$^{16}O + ^{150}Nd$	65	1.19	0.73	57.1	11.26	3.98	56.28	10.76	58.03

TABLE III. The energies and deformation values of the low-lying 2^+, 3^-, and 4^+ states for the interacting nuclei.

Reaction	Nucleus	Type	λ^π	E^* (MeV)	β_λ	Ref.
$^{16}O+^{142}Nd$	^{142}Nd	Vib	2^+	1.575	0.092	[61]
		Vib	3^-	2.084	0.127	[61]
	^{16}O	Vib	3^-	6.129	0.733	[62]
$^{16}O+^{150}Nd$	^{150}Nd	Rot	2^+	0.13	0.285	[63]
		Rot	4^+	0.381	0.05	[61]

The vibrational levels of the projectile do not seem to play any significant role in the sub-barrier fusion cross sections in this reaction. Instead, coupling of the 3^- state at 6.1 MeV of ^{16}O is found to overestimate the fusion cross sections, as shown by the orange dot-dashed-dotted line in Fig. 5. It is interesting to see that the coupling scheme required for the $^{16}O+^{142}Nd$ reaction is similar to that reported for the $^{16}O+^{144}Sm$ reaction [12] at sub-barrier energies.

2. $^{16}O+^{150}Nd$ *reaction*

Compared with the $^{16}O+^{142}Nd$ reaction, the degree of enhancement of sub-barrier fusion cross sections is high in $^{16}O+^{150}Nd$ reaction. ^{150}Nd is a deformed nucleus having a well-developed ground state rotational band with quadrupole deformation parameter (β_2) of 0.285 and hexadecupole deformation (β_4) of 0.05 [61]. The coupling of the first-excited state (2^+) significantly enhances the sub-barrier cross sections in this case, as shown in Fig. 6. The coupling of 2^+ and 4^+ states together reproduces the experimental cross sections quite well, as shown by the dot-dashed line in the same figure. ER cross sections reported in a previous study [64] is also shown in the same figure.

It is observed that the CC calculations using standard AW parameters fail to reproduce the experimental fusion cross sections at $E > 80$ MeV in both reactions in this work. A part of the excitation function, where the deviation from the CCFULL calculation is significant, is shown in Figs. 7(a) and 7(b). The cross sections are shown on a linear scale here. The deviation is observed to increase with increasing beam energy. A similar trend in cross sections at high excitation energies has been noticed in some other systems [37]. This aspect is discussed in the next section.

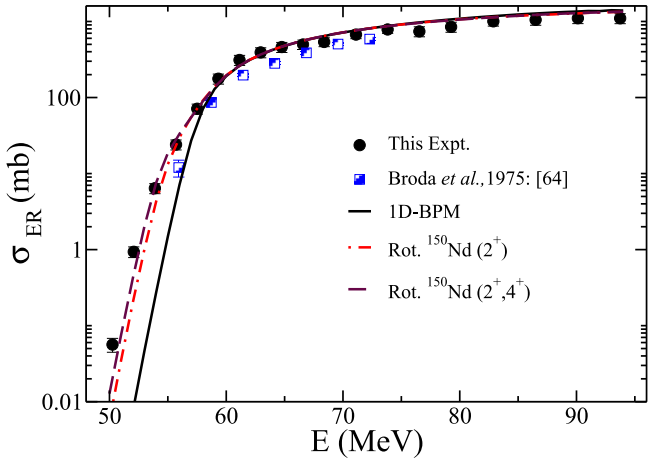

FIG. 6. The experimental fusion excitation function for the $^{16}O+^{150}Nd$ reaction along with CC calculations.

B. Potential parameters at energies well above the barrier

The inadequacy of AW potential parameters in CC calculations to describe fusion at well-above-barrier energies is not unique to the present systems. A similar trend has been reported for the $^{16}O+^{144,148,154}Sm$, $^{17}O+^{144}Sm$, $^{16}O+^{186}W$ [12], and $^{16}O+^{208}Pb$ [43] reactions. Capture cross-section studies in $^{40}Ca+^{186}W$ and $^{40}Ca+^{192}Os$ [65], ^{48}Ca, ^{50}Ti, and ^{54}Cr on ^{208}Pb [66] also reported a similar trend of cross sections at higher energies.

The difference observed in the measured and theoretical cross sections increases with increasing excitation energy.

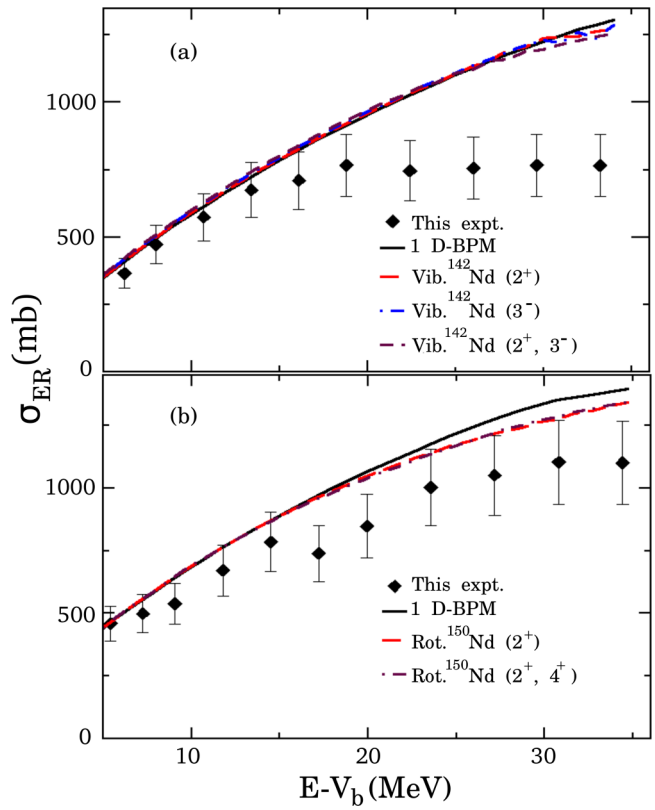

FIG. 7. (a) Plot of σ_{ER} (on linear scale) for $^{16}O+^{142}Nd$ reaction against the center-of-mass energy in excess of the barrier. Only cross sections at above-barrier energies are shown here. (b) Similar plot for $^{16}O+^{150}Nd$ reaction is shown.

TABLE IV. Calculated fission yields and sum of relative population of α channels at highest three beam energies (E_{beam}) in MeV.

	$^{16}O + ^{142}Nd$		$^{16}O + ^{150}Nd$	
E_{beam} (MeV)	$\Sigma\alpha$ (%)	σ_{fis} (%)	$\Sigma\alpha$ (%)	σ_{fis} (%)
104	28	<1	7	<1
100	22	<1	6.5	<1
96	20	<1	5.5	<1

As the fusion cross section is the sum of ER cross section and fission cross section, it is important to check whether the observed difference is due to the fission events that are not detected in this experiment. To rule out this possibility, PACE [55] calculations have been carried out at a few energy points where difference in the cross sections is noticed. The model parameters were fixed by reproducing the experimental fusion cross sections at near-barrier energies, where fission is negligible [57]. It has been observed that the calculated fission cross sections are negligibly small in the energy range of the present study for both systems. Fission becomes significant only at very high excitation energies in these reactions. A previous study on fission cross sections [57] reported that fission is significant at beam energies above 140 MeV for the $^{16}O + ^{142}Nd$ reaction.

Evaporation of α particles during the decay of the CN can also lead to a discrepancy in the experimental and theoretical total fusion cross sections, unless they are properly accounted for. α-particle emission becomes increasingly probable with increasing excitation energy of the CN. Some of the ERs, after the α emission, may escape from the acceptance of HIRA due to their larger recoil angle compared with the ERs produced by evaporating light particles such as neutrons, protons, etc. This might lead to decreased total ER cross sections if alpha emissions are not properly taken into account. We verified whether such alpha channels [55] contribute to the observed difference in the calculated and measured fusion cross sections in the present study. Calculated fission and the sum of various alpha channels for the two reactions (in percentage) are presented in Table IV for three beam energies where the experimental fusion cross sections showed significant deviation from CC calculations. It is observed that the contribution of α-particle evaporation cannot explain the huge difference in the calculated and experimental total fusion cross sections observed in this study.

It is known that the barrier distributions and the fusion cross sections cannot be reproduced simultaneously [43] using the standard AW potential parameters at very high excitation energies. A larger value of the diffuseness parameter was required to reproduce the fusion cross sections at such energies, compared with the average value ($\approx$0.65 fm) extracted from elastic-scattering data. We explored for an optimum set of potential parameters which could explain the cross sections consistently, across the energy range of present study, reasonably well. For this, the following method is adopted—the potential depth V_0 is chosen in such a way that it accommodates and absorbs all the partial waves. The parameters r_0 and

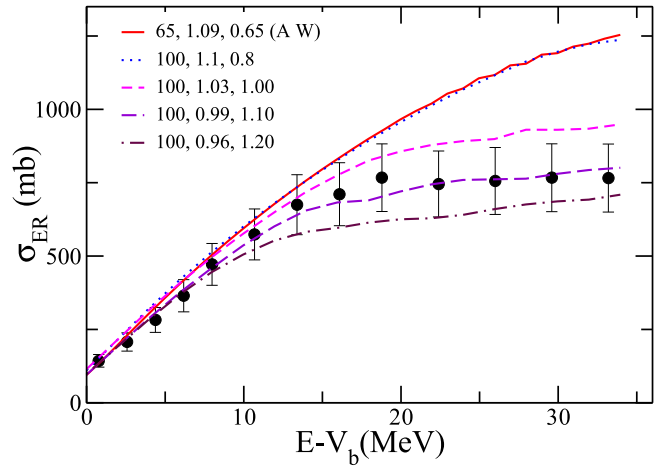

FIG. 8. Experimental fusion cross sections (on linear scale) compared with calculations using different V_0 (MeV), r_0 (fm), and a (fm) values, for the $^{16}O + ^{142}Nd$ reaction. A calculation using AW parametrization is shown with the solid red line.

a are then varied until the experimental barrier is reproduced, without any coupling to the internal degrees of freedom. Next, we introduced the couplings (vibrational coupling of ^{142}Nd in the case of $^{16}O + ^{142}Nd$ reaction and rotational coupling of ^{150}Nd in $^{16}O + ^{150}Nd$ reaction) and the potential parameters were once again adjusted to match the experimental barrier. The calculated cross sections for different sets of r_0 and a values (with V_0 frozen at 100 MeV) for the $^{16}O + ^{142}Nd$ at energies above the barrier are shown in Fig. 8, where the cross sections are shown on a linear scale. The parameter set V_0, r_0, and a that yields the lowest total χ^2 value has been chosen as the best set, and are 100 MeV, 0.99 fm, and 1.10 fm for the reaction $^{16}O + ^{142}Nd$ and 100 MeV, 1.04 fm, and 1.04 fm for the reaction $^{16}O + ^{150}Nd$.

Note that the optimum set obtained in this method reproduces the cross sections reasonably well in the entire energy range of the present study. However, deviations from experimental cross sections have been noticed at the lowest energy. The inability of the optimum set obtained from above-barrier cross sections to explain deep sub-barrier data has been noticed elsewhere [37]. Hence, with the limited data in the sub-barrier region we cannot comment about the suitability of these parameters at deep sub-barrier energies and warrant precise deep sub-barrier fusion measurements for these systems. The diffuseness parameters obtained for the two reactions are substantially larger than the AW parameters, similar to other cases [12,43].

C. Reactions forming ^{166}Er

In Fig. 9 we compare the reduced fusion cross sections of $^{16}O + ^{150}Nd$ and $^{18}O + ^{148}Nd$ reactions populating the same CN ^{166}Er. ER cross sections from Ref. [64] are also shown in the same figure. Despite having a positive Q-value neutron transfer channel ($2n$ stripping), the $^{18}O + ^{148}Nd$ reaction shows lower or comparable fusion cross sections at near-barrier energies.

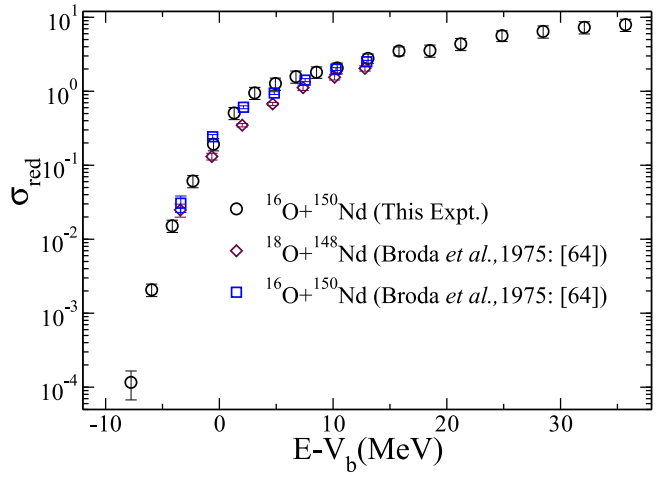

FIG. 9. Comparison of the reduced fusion cross sections forming the same CN (^{166}Er); the reaction ^{18}O + ^{148}Nd has a positive Q value for 2n-stripping channel.

It is established that one-neutron and two-neutron transfer channels with positive Q values have a major effect on the sub-barrier fusion enhancement [17,18,67]. A possible reason for the observed difference in reduced fusion cross sections of ^{16}O + ^{150}Nd and ^{18}O + ^{148}Nd reactions could be the dominance of target deformation effects over the positive Q-value neutron transfer channels at near- and sub-barrier energies in these two reactions. The target ^{150}Nd ($\beta_2 = 0.286$) is significantly deformed compared with ^{148}Nd ($\beta_2 = 0.201$ [63]). It is also reported that the *rigidity* of the nucleus with respect to collective excitations is important for sub-barrier fusion enhancement due to neutron rearrangement [29].

D. General remarks on ^{16}O + ^{A}Nd and ^{16}O + ^{A}Sm reactions

In Fig. 10 we compare the fusion cross sections of ^{16}O with different isotopes of neodymium. As the coupling effects

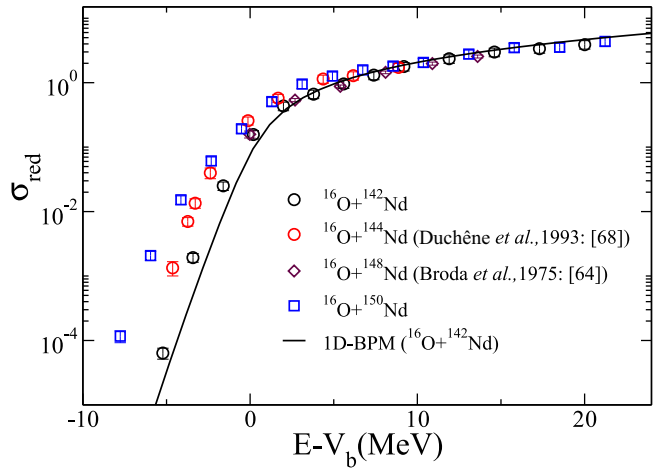

FIG. 10. Comparison of experimental fusion cross sections for the ^{16}O + ^{142,144,148,150}Nd reactions. The cross sections are converted to reduced scale by dividing the absolute cross section by $\pi\lambda\!\!\!^{-2}$ to remove the geometrical effects of the targets.

are important at sub- and near-barrier energies, cross sections above $E/V_b = 1.2$ are not considered for the comparison here. 1D-BPM calculations for the ^{16}O + ^{142}Nd reaction are shown as a reference in the same plot.

A systematic increase in fusion cross section with increasing neutron number in the target nucleus is seen at sub- and near-barrier energies. The enhancement is the highest in the ^{16}O + ^{150}Nd reaction and the least in the ^{16}O + ^{142}Nd reaction. For the ^{16}O + ^{148}Nd reaction, cross-section data at sub-barrier energies are not available. The fusion cross section for the reaction ^{16}O + ^{144}Nd is taken from Duchêne *et al.* [68]. A similar systematic behavior in fusion cross section was noticed in ^{16}O + ^{A}Sm reactions [12,69]. The varying collectivity of the nuclei along the isotopic chain of the targets used in these reactions is understood to be a major reason for this systematic behavior in these reactions [12].

Significant variation observed in the diffuseness parameter for the O + Sm systems ($a = 0.75$ fm for ^{16}O + ^{144}Sm, $a = 0.99$ fm for ^{16}O + ^{148}Sm, and $a = 1.06$ fm for the ^{16}O + ^{154}Sm reactions) was attributed to the increasing neutron number in the target nucleus in a previous study [44]. Such a large variation in the "a" value is not found in ^{16}O + ^{142}Nd and ^{16}O + ^{150}Nd reactions. A slightly larger a value is required for the reaction, using heavier target isotope, in this work too. However, conclusive remarks on the role of neutron excess in the target nuclei cannot be made in this case, considering the different α-evaporation cross sections for the two reactions.

E. Dynamical treatment of fusion

The failure of Akyüz-Winther potentials to reproduce capture cross sections has been noticed in many heavy systems. A larger value of the diffuseness parameter was required to fit the capture cross sections in reactions populating isotopes of curium [70]. Similar results were also reported in ^{40}Ca + ^{186}W and ^{40}Ca + ^{192}Os systems populating ^{226}Pu and ^{232}Cm [65], respectively. A similar observation was also made in reactions using heavy projectiles with ^{208}Pb [66]. In all these cases, deep-inelastic collisions (DICs) and quasifission [65,71,72] are dominant.

Both quasifission and DIC probability increase with the charge product $Z_P Z_T$. These processes could partially explain the observed inadequacy of AW parametrization to fit the capture or fusion cross sections in heavy systems with large $Z_p Z_T$ values. However, no quasifission is reported for the O + Sm or O + Nd reactions. Having very low $Z_p Z_T$ values, quasifission is expected to be negligibly small in these reactions. Hence, the observed deviation from AW potential parameters in these light, asymmetric reactions points toward the role of dynamical effects in fusion at high energies.

Although a possible role of dynamical effects in hindering fusion at very high energies was speculated more than a decade back, no remarkable progress has been made in this direction yet, particularly in heavy ion fusion theories. Along with other available data sets, the present data strongly call for a robust theoretical formalism, including the dynamical effects, to understand fusion of heavy nuclei.

V. SUMMARY AND CONCLUSION

Fusion cross sections have been measured for the $^{16}O + ^{142,150}Nd$ systems from 12% below to 50% above the Coulomb barrier, using HIRA. Fusion enhancement over 1D-BPM calculations has been noticed in both the systems.

CC calculations have been performed for both systems to explain the experimental results. Nuclear potential parameters V_0, r_0, and a were first fixed using the Akyüz-Winther parametrization. Vibrational coupling of 2^+ and 3^- states of ^{142}Nd is found to explain the sub-barrier fusion enhancement in the $^{16}O + ^{142}Nd$ reaction. Vibrational effects of ^{16}O seem to play no role in sub-barrier fusion in this reaction.

The degree of fusion enhancement is larger for the $^{16}O + ^{150}Nd$ reaction, compared with $^{16}O + ^{142}Nd$. Rotational couplings of (2^+ and 4^+ states) of the deformed target reproduced the fusion cross sections reasonably well in the $^{16}O + ^{150}Nd$ reaction at sub- and near-barrier energies. While the coupling schemes in the $^{16}O + ^{142}Nd$ reaction is similar to that of $^{16}O + ^{144}Sm$, the $^{16}O + ^{150}Nd$ reaction exhibits similarity with $^{16}O + ^{154}Sm$ reaction at near- and sub-barrier energies.

The role of collectivity in sub-barrier fusion enhancement is visible in the systematic enhancement of fusion cross sections in reactions with different isotopes of Nd. A comparison of $^{16}O + ^{150}Nd$ and $^{18}O + ^{148}Nd$ systems do not show any special effects of transfer channels in the latter reaction, even though the system has positive Q- value for the two-neutron transfer (stripping) reaction.

Although CC calculations assuming AW potential parameters reasonably reproduce the fusion cross sections at below-barrier energies, they overpredict fusion at energies well above the barrier. This difference is observed to increase with increasing beam energy. Careful analysis indicates that the observed difference is not due to fission or α-particle emission. A diffuseness parameter in the range 1.0–1.1 fm is required to fit the cross sections. These values are significantly larger than the values obtained from elastic-scattering measurements.

The diffuseness parameter required to fit the higher-energy cross sections does not differ significantly in the two reactions. The slight difference observed in the value of a may not be attributed to the neutron number difference because the calculated α evaporation probability for the two reactions vary significantly at similar excitation energy.

The inadequacy of AW potential parameters hints at the role of dynamical effects in fusion at higher energies. The present study strongly recommends a revised theoretical approach incorporating dynamical effects to understand heavy ion fusion.

ACKNOWLEDGMENTS

We are thankful to the accelerator staff of IUAC for providing excellent beams throughout the experiment. Support received from the data support lab is also highly acknowledged. A.C.V. and S.M. gratefully acknowledge Kerala State Council for Science Technology and Environment (KSCSTE) for financial support in the form of a fellowship. Illuminating discussions with K. Hagino are highly acknowledged.

[1] Y. T. Oganessian and V. K. Utyonkov, Rep. Prog. Phys. **78**, 036301 (2015).
[2] K. Morita *et al.*, J. Phys. Soc. Jpn. **76**, 043201 (2007).
[3] Y. T. Oganessian *et al.*, J. Phys. G **34**, R165 (2007).
[4] S. Hofmann and G. Munzenberg, Rev. Mod. Phys. **72**, 733 (2000).
[5] N. Bohr and J. A. Wheeler, Phys. Rev. **56**, 426 (1939).
[6] A. B. Balantekin and N. Takigawa, Rev. Mod. Phys. **70**, 77 (1998).
[7] M. Dasgupta, D. J. Hinde, N. Rowley, and A. M. Stefanini, Annu. Rev. Nucl. Part. Sci. **48**, 401 (1998).
[8] B. B. Back, H. Esbensen, C. L. Jiang, and K. E. Rehm, Rev. Mod. Phys. **86**, 317 (2014).
[9] M. Beckerman, Rep. Prog. Phys. **51**, 1047 (1988).
[10] W. Reisdorf *et al.*, J. Phys. G **20**, 1297 (1994).
[11] R. G. Stokstad and E. E. Gross, Phys. Rev. C **23**, 281 (1981).
[12] J. R. Leigh, M. Dasgupta, D. J. Hinde, J. C. Mein, C. R. Morton, R. C. Lemmon, J. P. Lestone, J. O. Newton, H. Timmers, J. X. Wei, and N. Rowley, Phys. Rev. C **52**, 3151 (1995).
[13] J. D. Bierman, P. Chan, J. F. Liang, M. P. Kelly, A. A. Sonzogni, and R. Vandenbosch, Phys. Rev. Lett. **76**, 1587 (1996).
[14] A. M. Stefanini, D. Ackermann, L. Corradi, J. H. He, G. Montagnoli, S. Beghini, F. Scarlassara, and G. F. Segato, Phys. Rev. C **52**, R1727 (1995).
[15] J. O. Newton, C. R. Morton, M. Dasgupta, J. R. Leigh, J. C. Mein, D. J. Hinde, H. Timmers, and K. Hagino, Phys. Rev. C **64**, 064608 (2001).
[16] A. M. Stefanini, D. Ackermann, L. Corradi, D. R. Napoli, C. Petrache, P. Spolaore, P. Bednarczyk, H. Q. Zhang, S. Beghini, G. Montagnoli, L. Mueller, F. Scarlassara, G. F. Segato, F. Soramel, and N. Rowley, Phys. Rev. Lett. **74**, 864 (1995).
[17] V. I. Zagrebaev, Phys. Rev. C **67**, 061601(R) (2003).
[18] V. Tripathi, L. T. Baby, J. J. Das, P. Sugathan, N. Madhavan, A. K. Sinha, P. V. MadhusudhanaRao, S. K. Hui, R. Singh, and K. Hagino, Phys. Rev. C **65**, 014614 (2001).
[19] L. T. Baby, V. Tripathi, D. O. Kataria, J. J. Das, P. Sugathan, N. Madhavan, A. K. Sinha, M. C. Radhakrishna, N. M. Badiger, N. G. Puttaswamy, A. M. Vinodkumar, and N. V. S. V. Prasad, Phys. Rev. C **56**, 1936 (1997).
[20] N. Rowlay, G. R. Satchler, and P. H. Stelson, Phys. Lett. B **254**, 25 (1991).
[21] A. M. Stefanini, L. Corradi, A. M. Vinodkumar, Yang Feng, F. Scarlassara, G. Montagnoli, S. Beghini, and M. Bisogno, Phys. Rev. C **62**, 014601 (2000); **65**, 034609 (2002).
[22] O. A. Capurro, J. E. Testoni, D. Abriola, D. E. DiGregorio, J. O. Fernández Niello, G. V. Martí, A. J. Pacheco, M. R. Spinella, M. Ramírez, C. Balpardo, and M. Ortega, Phys. Rev. C **65**, 064617 (2002).

[23] R. A. Broglia, C. H. Dasso, S. Landowne, and A. Winther, Phys. Rev. C **27**, 2433 (1983).

[24] R. A. Broglia, C. H. Dasso, S. Landowne, and G. Pollarolo, Phys. Lett. B **133**, 34 (1983).

[25] J. J. Kolata, A. Roberts, A. M. Howard, D. Shapira, J. F. Liang, C. J. Gross, R. L. Varner, Z. Kohley, A. N. Villano, H. Amro, W. Loveland, and E. Chavez, Phys. Rev. C **85**, 054603 (2012).

[26] F. Scarlassara, S. Beghini, G. Montagnoli, G. F. Segato, D. Ackermann, L. Corradi, C. J. Lin, A. M. Stefanini, and L. F. Zheng, Nucl. Phys. A **672**, 99 (2000).

[27] A. M. Stefanini, B. R. Behera, S. Beghini, L. Corradi, E. Fioretto, A. Gadea, G. Montagnoli, N. Rowley, F. Scarlassara, S. Szilner, and M. Trotta, Phys. Rev. C **76**, 014610 (2007).

[28] Z. Kohley, J. F. Liang, D. Shapira, R. L. Varner, C. J. Gross, J. M. Allmond, A. L. Caraley, E. A. Coello, F. Favela, K. Lagergren, and P. E. Mueller, Phys. Rev. Lett. **107**, 202701 (2011).

[29] V. A. Rachkov, A. V. Karpov, A. S. Denikin, and V. I. Zagrebaev, Phys. Rev. C **90**, 014614 (2014).

[30] H. M. Jia, C. J. Lin, F. Yang, X. X. Xu, H. Q. Zhang, Z. H. Liu, L. Yang, S. T. Zhang, P. F. Bao, and L. J. Sun, Phys. Rev. C **86**, 044621 (2012).

[31] V. V. Sargsyan, G. G. Adamian, N. V. Antonenko, W. Scheid, and H. Q. Zhang, Phys. Rev. C **84**, 064614 (2011).

[32] G. L. Zhang, X. X. Liu, and C. J. Lin, Phys. Rev. C **89**, 054602 (2014).

[33] A. A. Ogloblin, H. Q. Zhang, C. J. Lin, H. M. Jia, S. V. Khlebnikov, E. A. Kuzmin, W. H. Trzaska, X. X. Xu, F. Yan, V. V. Sargsyan, G. G. Adamian, N. V. Antonenko, and W. Scheid, Eur. Phys. J. A **50**, 157 (2014).

[34] C. L. Jiang, H. Esbensen, K. E. Rehm, B. B. Back, R. V. F. Janssens, J. A. Caggiano, P. Collon, J. Greene, A. M. Heinz, D. J. Henderson, I. Nishinaka, T. O. Pennington, and D. Seweryniak, Phys. Rev. Lett. **89**, 052701 (2002); **93**, 012701 (2004); Phys. Rev. C **71**, 044613 (2005); **78**, 017601 (2008).

[35] A. M. Stefanini, G. Montagnoli, R. Silvestri, S. Beghini, L. Corradi, S. Courtin, E. Fioretto, B. Guiot, F. Haas, D. Lebhertz, N. Mărginean, P. Mason, F. Scarlassara, R. N. Sagaidak, and S. Szilner, Phys. Rev. C **78**, 044607 (2008).

[36] G. Montagnoli, A. M. Stefanini, C. L. Jiang, H. Esbensen, L. Corradi, S. Courtin, E. Fioretto, A. Goasduff, F. Haas, A. F. Kifle, C. Michelagnoli, D. Montanari, T. Mijatovic, K. E. Rehm, R. Silvestri, P. P. Singh, F. Scarlassara, S. Szilner, X. D. Tang, and C. A. Ur, Phys. Rev. C **85**, 024607 (2012).

[37] M. Dasgupta, D. J. Hinde, A. Diaz-Torres, B. Bouriquet, C. I. Low, G. J. Milburn, and J. O. Newton, Phys. Rev. Lett. **99**, 192701 (2007).

[38] Ş. Mişicu and H. Esbensen, Phys. Rev. Lett. **96**, 112701 (2006); Phys. Rev. C **75**, 034606 (2007).

[39] C. H. Dasso and G. Pollarolo, Phys. Rev. C **68**, 054604 (2003).

[40] C. Simenel, A. S. Umar, K. Godbey, M. Dasgupta, and D. J. Hinde, Phys. Rev. C **95**, 031601(R) (2017).

[41] T. Ichikawa, K. Hagino, and A. Iwamoto, Phys. Rev. C **75**, 057603 (2007); Phys. Rev. Lett. **103**, 202701 (2009).

[42] A. Diaz-Torres, D. J. Hinde, M. Dasgupta, G. J. Milburn, and J. A. Tostevin, Phys. Rev. C **78**, 064604 (2008); **81**, 041603(R) (2010).

[43] C. R. Morton, A. C. Berriman, M. Dasgupta, D. J. Hinde, J. O. Newton, K. Hagino, and I. J. Thompson, Phys. Rev. C **60**, 044608 (1999).

[44] J. O. Newton, R. D. Butt, M. Dasgupta, D. J. Hinde, I. I. Gontchar, C. R. Morton, and K. Hagino, Phys. Lett. B **586**, 219 (2004); Phys. Rev. C **70**, 024605 (2004).

[45] A. Mukherjee, D. J. Hinde, M. Dasgupta, K. Hagino, J. O. Newton, and R. D. Butt, Phys. Rev. C **75**, 044608 (2007).

[46] I. I. Gontchar, D. J. Hinde, M. Dasgupta, and J. O. Newton, Phys. Rev. C **69**, 024610 (2004).

[47] K. Hagino, N. Rowley, and M. Dasgupta, Phys. Rev. C **67**, 054603 (2003).

[48] K. Hagino, T. Takehi, A. B. Balantekin, and N. Takigawa, Phys. Rev. C **71**, 044612 (2005).

[49] K. Washiyama, K. Hagino, and M. Dasgupta, Phys. Rev. C **73**, 034607 (2006).

[50] D. Kanjilal, S. Chopra, M. M. Narayanan, Indira S. Iyer, Vandana Jha, R. Joshi, and S. K. Datta, Nucl. Instrum. Methods Phys. Res., Sect. A **328**, 97 (1993).

[51] A. K. Sinha, N. Madhavan, J. J. Das, P. Sugathan, D. O. Kataria, A. P. Patro, and G. K. Mehta, Nucl. Instrum. Methods Phys. Res., Sect. A **339**, 543 (1994).

[52] J. Gehlot, Ph.D. thesis, Calicut University, 2019 (unpublished); http://hdl.handle.net/10603/307463

[53] S. Nath, P. V. M. Rao, S. Pal, J. Gehlot, E. Prasad, G. Mohanto, S. Kalkal, J. Sadhukhan, P. D. Shidling, K. S. Golda, A. Jhingan, N. Madhavan, S. Muralithar, and A. K. Sinha, Phys. Rev. C **81**, 064601 (2010).

[54] S. Nath, Comput. Phys. Commun. **180**, 2392 (2009).

[55] A. Gavron, Phys. Rev. C **21**, 230 (1980).

[56] T. Rajbongshi, K. Kalita, S. Nath, J. Gehlot, T. Banerjee, I. Mukul, R. Dubey, N. Madhavan, C. J. Lin, A. Shamlath, P. V. Laveen, M. Shareef, N. Kumar, P. Jisha, and P. Sharma, Phys. Rev. C **93**, 054622 (2016).

[57] A. Gavron, J. Boissevain, H. C. Britt, K. Eskola, P. Eskola, M. M. Fowler, H. Ohm, J. B. Wilhelmy, T. C. Awes, R. L. Ferguson, F. E. Obenshain, F. Plasil, G. R. Young, and S. Wald, Phys. Rev. C **30**, 1550 (1984).

[58] K. Hagino, N. Rowley, and A. T. Kruppa, Comput. Phys. Commun. **123**, 143 (1999).

[59] R. A. Broglia and A. Winther, *Heavy Ion Reaction Lecture Notes, Vol. 1: Elastic and Inelastic Reactions* (Benjamin Cummings, Reading, 1981).

[60] W. J. Swiatecki, K. Siwek-Wilczynska, and J. Wilczynski, Phys. Rev. C **71**, 014602 (2005).

[61] M. Pignanelli, N. Blasi, J. A. Bordewijk, R. De Leo, M. N. Harakeh, M. A. Hofstee, S. Micheletti, R. Perrino, V. Yu. Ponomarev, V. G. Soloviev, A. V. Sushkov, and S. Y. van der Werf, Nucl. Phys. A **559**, 1 (1993).

[62] G. M. Crawley and G. T. Garvey, Phys. Rev. **160**, 981 (1967).

[63] S. Raman, C. W. Nestor, Jr., and P. Tikkanen, At. Data Nucl. Data Tables **78**, 1 (2001).

[64] R. Broda, M. Ishihara, B. Herskind, H. Oeschler, S. Ogaza, and H. Ryde, Nucl. Phys. A **248**, 356 (1975).

[65] E. Prasad, D. J. Hinde, E. Williams, M. Dasgupta, I. P. Carter, K. J. Cook, D. Y. Jeung, D. H. Luong, C. S. Palshetkar, D. C. Rafferty, K. Ramachandran, C. Simenel, and A. Wakhle, Phys. Rev. C **96**, 034608 (2017).

[66] K. Banerjee, D. J. Hinde, M. Dasgupta, E. C. Simpson, D. Y. Jeung, C. Simenel, B. M. A. Swinton-Bland, E. Williams, I. P. Carter, K. J. Cook, H. M. David, Ch. E. Düllmann, J. Khuyagbaatar, B. Kindler, B. Lommel, E. Prasad, C. Sengupta, J. F. Smith, K. Vo-Phuoc, J. Walshe, and A. Yakushev, Phys. Rev. Lett. **122**, 232503 (2019).

[67] V. Yu. Denisov, Eur. Phys. J. A **7**, 87 (2000).
[68] G. Duchêne, P. Romain, F. A. Beck, Ph. Benet, D. Disdier, B. Haas, B. Lott, V. Rauch, F. Scheibling, J. P. Vivien, S. K. Basu, E. Bozek, K. Zuber, D. Di Gregorio, and J. Fernandez-Niello, Phys. Rev. C **47**, 2043 (1993).
[69] K. Hagino and N. Takigawa, Prog. Theor. Phys. **128**, 1061 (2012).
[70] E. Williams, D. J. Hinde, M. Dasgupta, R. du Rietz, I. P. Carter, M. Evers, D. H. Luong, S. D. McNeil, D. C. Rafferty, K. Ramachandran, and A. Wakhle, Phys. Rev. C **88**, 034611 (2013).
[71] W. J. Swiatecki, Phys. Scr. **24**, 113 (1981).
[72] J. P. Blocki, H. Feldmeier, and W. J. Swiatecki, Nucl. Phys. A **459**, 145 (1986).